



## Research Article

# The Creep Test Study and Macro-Detail Analysis of Argillaceous Red Sandstone in Different Water-Containing States

Shuntao Guo,<sup>1</sup> Shujie Wen ,<sup>1</sup> Hongyu Guo,<sup>2</sup> and Helin Fu <sup>3</sup>

<sup>1</sup>School of Civil Engineering and Surveying and Mapping Engineering, Jiangxi University of Science and Technology, Ganzhou, China

<sup>2</sup>China Construction Fifth Engineering Division Corp. Ltd, Changsha, China

<sup>3</sup>School of Civil Engineering, Central South University, Changsha, China

Correspondence should be addressed to Shujie Wen; [wenshujie@jxust.edu.cn](mailto:wenshujie@jxust.edu.cn) and Helin Fu; [fu.h.l@mail.csu.edu.cn](mailto:fu.h.l@mail.csu.edu.cn)

Received 17 December 2021; Revised 9 March 2022; Accepted 12 March 2022; Published 30 March 2022

Academic Editor: Qian Chen

Copyright © 2022 Shuntao Guo et al. This is an open access article distributed under the Creative Commons Attribution License, which permits unrestricted use, distribution, and reproduction in any medium, provided the original work is properly cited.

In order to study the creep characteristics and failure mechanism of argillaceous red sandstone in a water-bearing state, uniaxial creep tests of argillaceous red sandstone under dry and saturated states are carried out under fractional loading. Burgers model is used to fit the test results and identify the parameters, and scanning electron microscopy is carried out on the cross section of the damaged sample. The mechanism of creep difference of argillaceous red sandstone with different water content is studied from the microscopic point of view. The results show that the uniaxial compressive strength of the saturated clay red sandstone is 46% of that of the dry clay red sandstone. The deformation level of the saturated clay red sandstone is lower than that of the dry clay red sandstone. The limit deformation of the creep failure of the water-bearing clay red sandstone is much smaller than that of the dry clay red sandstone. The long-term strength of the muddy red sandstone is 46.4 MPa in the dry state and only 14.1 MPa in the saturated state, as calculated at the steady-state creep rate. It is found that the Burgers model can describe the attenuation and stable creep of muddy red sandstone well. Through macro- and microanalysis, it is found that the compression failure form of argillaceous red sandstone belongs to x-shaped conjugate inclined plane shear failure. After saturation, the internal pores of argillaceous red sandstone become larger, and the cementation ability decreases, resulting in the decrease of rock sample strength.

## 1. Introduction

The stability of the geotechnical body is an important prerequisite for the safety of geotechnical engineering [1]. Most of the rock engineering instability is due to the rheological damage caused by the gradual accumulation of damage inside the rock over time. Water as the main cause of various geological hazards is an important factor affecting the creep characteristics of rocks. This is more obvious for soft rocks, which are with high mud content and are easy to disintegrate and soften with water. If the influence of water on the creep properties of muddy red sandstone is ignored, it will cause huge engineering accidents. Many scholars have studied the creep properties of soft rocks [2–6] and the effect of water on the mechanical properties of soft rocks [7–10]. Baud et al. [11] performed triaxial compression tests on the

Berea, Boise, Darley Dale, and Gosford sandstones and found that the brittle strength of the rocks was reduced by 5–17% in the presence of water. Wu et al. [12] conducted graded loading creep experiments on salt rocks and established a viscoelastic-plastic damage creep model for salt rocks based on creep results, and the reasonableness of the model was further verified based on sensitivity analysis of the parameters. Zhang et al. [13] investigated the effect of saturation on the strength, elastic modulus, crack initiation stress, and damage stress threshold of siltstone. Yao et al. [14] found that the peak stress and elastic modulus in coal rocks decreased with increasing water content, but the closure stress, crack initiation stress, and damage stress thresholds did not change with increasing water content. Wang et al. [15] studied the triaxial creep behavior of the Brazilian Formation mudstone and obtained a model that

could accurately simulate the creep of the Brazilian Formation mudstone by improving the burgers model. Based on graded incremental addition and removal test, Ping et al. [16] found that the strength at destruction accounted for 57.6% of the uniaxial compressive strength for dry specimens and 86.5% for specimens in a water environment, with a low percentage of destruction strength at drying to compressive strength. Yu et al. [17] conducted uniaxial compression and multistage loading tests on red sandstone at different water contents and found that water can significantly reduce the elastic modulus of red sandstone, and the steady-state creep strain rate of dry, saturated, and soaked specimens increased with the stress level in a power law. Miyazaki [18] conducted creep tests on olivine and proposed a model based on Orowan's law to predict the creep strain rate under high temperature and low-stress states. Nadimi et al. [19] conducted a triaxial creep test on the surrounding rock in the cave of the hydropower station to estimate the deformation law of the surrounding rock of the cave and calculated the parameters of the surrounding rock creep model through the results of the creep test and the in-situ test. The validity of the parameters was verified. All the above results have advanced the study of creep properties of soft rocks, but there are few reports on the in-depth study of creep properties of muddy red sandstones in different water-bearing states and the macroscopic mechanism analysis of their variability.

This paper takes the muddy red sandstone at the construction site of the river crossing tunnel in Rongjiang New Area as the research object. The creep test with graded loading is performed under uniaxial compression of the muddy red sandstone in dry and full water state, and the creep characteristics of the muddy red sandstone in different water states are studied. Furthermore, electron microscope scanning on the damaged specimen section is performed to study the fine mechanism of the difference of creep characteristics of the muddy red sandstone in different water states. Through the creep curve, a suitable creep model is selected to fit the curve, and the rheological and mechanical parameters of the muddy red sandstone are obtained by nonlinear fitting. The parameters can be used for numerical simulation, which will provide data reference for engineering research and long-term operation.

## 2. Specimen Preparation and Test Equipment and Programs

**2.1. Specimen Preparation.** The muddy red sandstone tested was taken from the construction site of the river crossing tunnel in Rongjiang New Area, Ganzhou, Jiangxi. The specimens were drilled, cut, and polished into cylindrical specimens of  $\Phi 50 \text{ mm} \times 100 \text{ mm}$ , and the size of the specimens met the requirements of the "Engineering Rock Test Methods Standard". There were a large number of microfractures in the muddy red sandstone. In order to reduce the dispersion of the experimental results, the RSM-SY5 (*T*) nonmetallic acoustic detector was used to screen the polished specimens before the test [20]. Specimens with similar

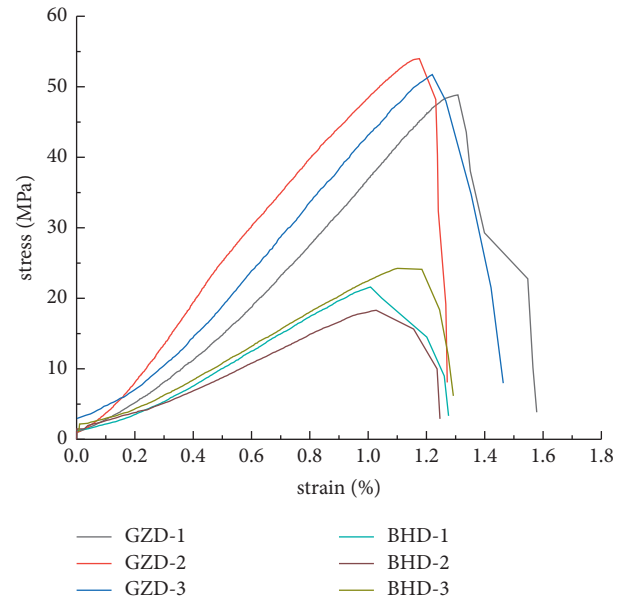


FIGURE 1: Uniaxial compressive stress-strain relationship curve.

wave speeds were selected, and the specimen for storage was sealed immediately after the test.

**2.2. Test Equipment.** The test was conducted using the RMT-150C rock mechanics testing machine developed by the Wuhan Institute of Geotechnics, Chinese Academy of Sciences. The strain was measured by applying strain gauges, the strain collector was ZI-120P, and a data collector was developed by Zhubang Measurement and Control. The collector was connected to a computer system and could store a large amount of data and view real-time curves with a minimum acquisition interval of 1 s. The acquisition interval was set as 1 s for the uniaxial compression test and 30 s for the creep test in order to prevent too much data.

**2.3. Test Protocols.** Since the rocks at the entrance of the river tunnel were close to the air-dry state, and the rocks at the bottom of the river were in the water-saturated state, and 12 specimens were selected and divided into 4 groups, including 2 groups of specimens in the dry state and 2 groups of specimens in the water-saturated state, for uniaxial compression tests and uniaxial compression creep tests, in order to obtain reasonable parameters as far as possible. The compressive strength of the specimens was tested by a uniaxial compression test, and the stress-strain curves were obtained (Figure 1). The basic physical and mechanical parameters of the specimens in dry and water-filled states are shown in Table 1. Due to the physical and chemical softening effect of water on muddy red sandstone, the strength of muddy red sandstone in the water-saturated state was only about half of that in the dry state. The uniaxial compression test yielded a peak stress of 51.4 MPa for muddy red sandstone in the dry state and 23.9 MPa in the water-saturated state. The first stage was taken as 40% of the peak

TABLE 1: Physical and mechanical parameters of argillaceous red sandstone samples.

Water content status	Density (g/cm <sup>3</sup> )	Compression strength (MPa)	Elastic modulus (GPa)	Poisson's ratio	Wave velocity	Porosity	Softening factor
Drying	2.49	51.4	6.03	0.33	2633	9.01%	—
Saturated	2.55	23.9	2.29	0.40	2532	—	0.46

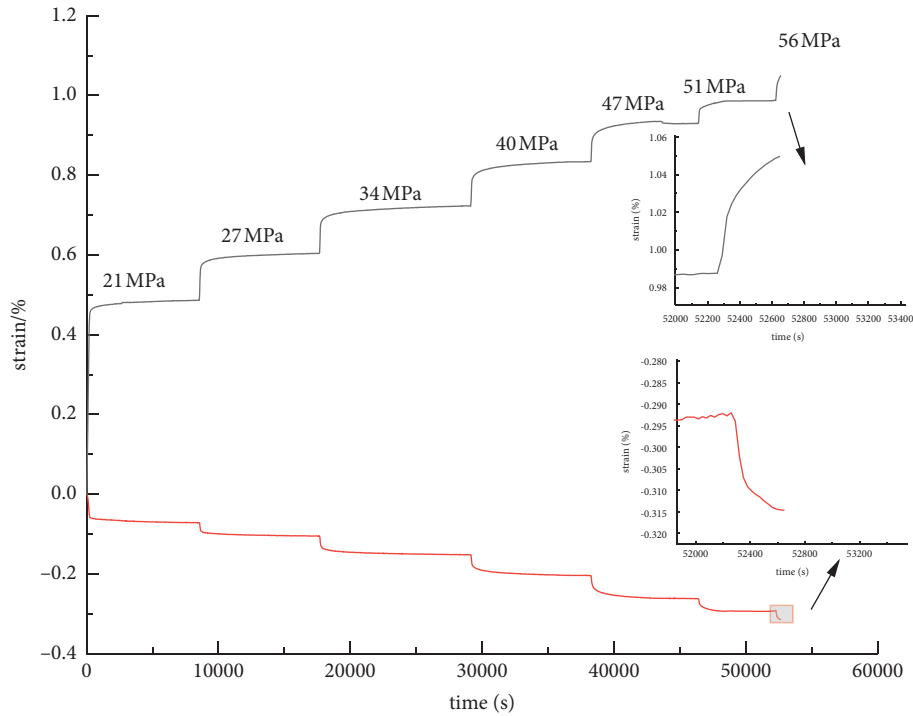


FIGURE 2: Creep curves of specimens in a dry state.

stress, and each stage was increased by 10% until the specimen was damaged. The creep duration was 2.5 hours.

### 3. Analysis of Test Results

The full ephemeral creep curves of muddy red sandstone in dry and water-filled states were obtained by graded loading creep tests, as shown in Figures 2 and 3.

As can be seen from Figure 2, the creep characteristics of the specimen and the loaded stress were closely related. Taking the specimen in the dry state as an example, when the axial differential stress increased from 21 MPa to 51 MPa, the axial strain increased by 0.5%, and the lateral strain increased by 0.222%. Meanwhile, the stress of the first stage loading is 40% of the peak stress; that is, the axial compression strain has reached 49% of the strain at destruction after the stress gradient increases from 0 MPa to 21 MPa. This indicates that most of the microfractures in the rock have closed during the first stage stress increase, which results in a sharp increase in strain, while the increase in lateral strain is not as pronounced.

As shown in Figure 3, the axial stress of the water-filled specimen was applied from 0 MPa to 12 MPa and stabilized at 12 MPa when the axial strain was stabilized at 0.487%, about 69% of the damage strain, and the lateral strain was

stabilized at 0.214%, about 77% of the strain at the damage, and the damage started at the third level of stress.

Compared with the specimens in the dry state, the stresses generated by the first stage of loading and the deformation at the time of damage were accounted for a larger proportion of the deformation of the specimens in the water-saturated state. Both two specimens produced a deformation of about 0.49% under the first stage of stress, but the stresses on the water-saturated specimens were only half of those in the dry state. This is because the fissures in the specimen become larger and gradually penetrate after filling with water, increasing the damage to the specimen, so the rock is more likely to be deformed when squeezed by external forces [21, 22].

The long-term strength of rocks is a stress limit to distinguish stable creep and unstable creep of rocks [23], beyond which the creep of rocks proceeds toward unstable creep. It can be seen from Figures 4 and 5 that under the action of low stress, the steady-state rate of rock sample increases slowly with the increase of stress. When the stress value exceeds the long-term strength, the creep rate increases rapidly. Steady-state creep rate increases exponentially with increasing stress. In this paper, the long-term strength of the rock is derived from the steady-state rate (Figures 4 and 5), and it can be seen from the figure that the

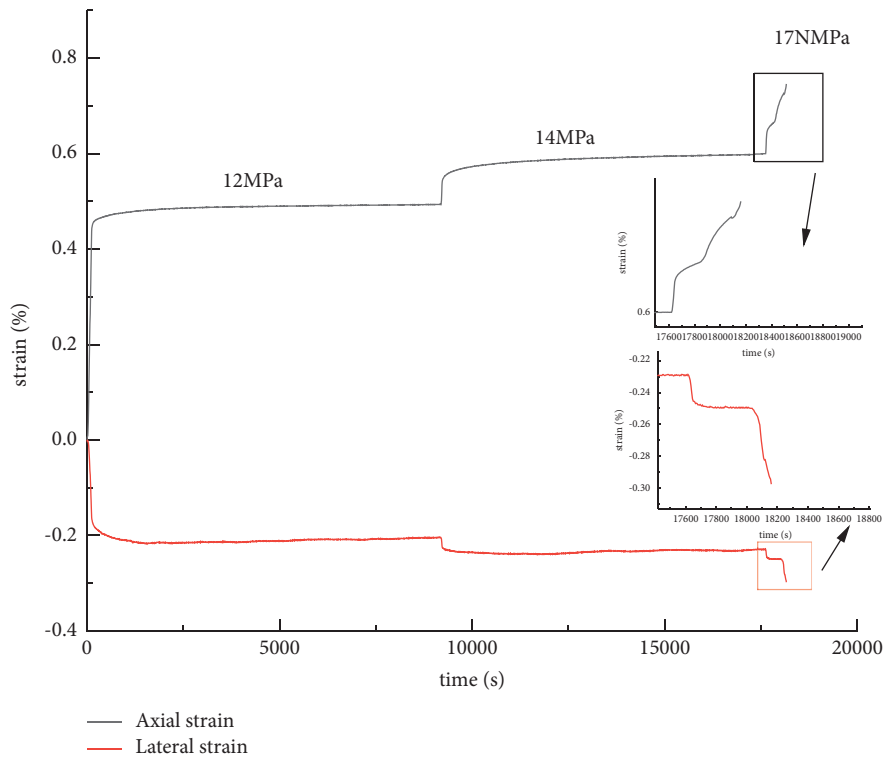


FIGURE 3: Creep curves of specimens in a saturated state.

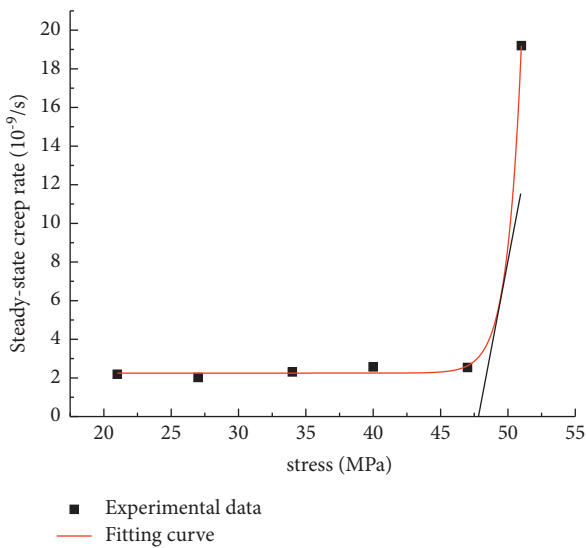


FIGURE 4: Creep rate-stress curve of specimens in a dry state.

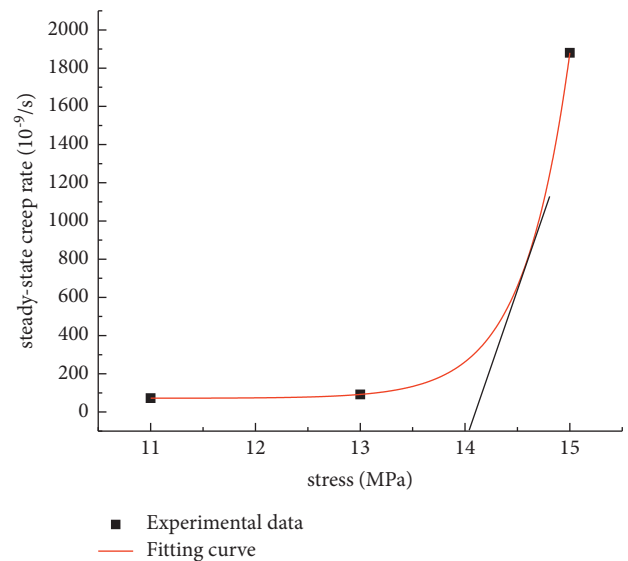


FIGURE 5: Creep rate-stress curve of specimens in a saturated state.

uniaxial long-term strength of the muddy red sandstone in the dry state is about 46.4 MPa, and the long-term strength in the saturated state is about 14.1 MPa. It can be seen that water has a great influence on the strength of the muddy red sandstone, and the long-term strength in the saturated state is only about 30% of that in the dry state.

#### 4. Creep Model and Parameter Identification

4.1. *The Burgers Model.* From the creep experimental curves, it can be seen that the muddy red sandstone exhibits obvious viscoelasticity and transient elasticity under all levels of stress. Burgers model, which consists of Maxwell body and

Kelvin body in series, can describe these properties well, as shown in Figure 6.

For Maxwell bodies, the instanton equation is  $\sigma + \beta/E\dot{\sigma} = \beta\dot{\varepsilon}$ , and the creep equation is  $\varepsilon(t) = \sigma_0/E + \sigma_0/\beta t$ . For Kelvin bodies, the instanton equation is  $\sigma = E\varepsilon + \beta\dot{\varepsilon}$ , and the creep equation is  $\varepsilon(t) = \sigma_0/E[1 - e^{(-E/\beta)t}]$ .

By connecting  $K$  and  $M$  bodies in series, the creep equation of the burgers model can be obtained after a series of computational transformations of the equation [24].

$$\varepsilon(t) = \frac{\sigma_0}{E_1} + \frac{\sigma_0}{\beta_1}t + \frac{\sigma_0}{E_2} \left(1 - e^{(-E_2t/\beta_2)}\right), \quad (1)$$

where  $E_1$  and  $E_2$  are elastic coefficients;  $\beta_1$  and  $\beta_2$  are Newtonian viscosity coefficients; and  $\sigma_0$  is the stress at all levels of graded loading.

From (1), it can be seen that at the instant of  $\sigma_0$  when the stress arrives, this is when  $t = 0$ ,  $\varepsilon(0) = \sigma_0/E_1$ , only the Hooke body  $E_1$  plays a role.

**4.2. Parameter Identification.** Boltzmann superposition principle was used to shift the coordinate of the creep test curve. With the help of Origin's custom function, the burgers model was added into Origin's function library, the creep curve under all levels of stress was fitted nonlinearly, and the parameters were identified by the Levenberg-Marquardt optimization algorithm. The resulting curves are shown in Figures 7 and 8, and each creep parameter is shown in Table 2.

From the fitting results of creep parameters in Table 2, it can be seen that the viscosity coefficients  $\beta_1$ ,  $\beta_2$  of the specimens in the dry state increase with the increase of stress level, indicating that the viscosity is increasing, while the viscosity coefficient in the saturated state decreases with the increase of stress instead. This is because the action of water reduces the cohesion between the rock particles, and the particles are easily separated as the stress increases.

The correlation coefficients of the creep curves fitted by the burgers model for all levels of stress are above 0.91, and the results show that the burgers creep model can well describe the creep properties of muddy red sandstone. The parameters obtained from the fitting can be used for numerical simulation at the same time, which has some application value for analyzing and studying the long-term stability of the project.

## 5. Macro- and Microanalysis of Failure Specimen

**5.1. Macroanalysis.** At the end of each test, the failure specimen fragments were collected and pieced back to the original shape as far as possible, and the fragments were fixed with adhesive tape. Figure 9 shows the specimens after uniaxial failure in the dry state and the water-filled state.

Regardless of the dry or waterlogged state of the failure specimen, there is a conical fragment at the top. The axial main fracture arises in the middle of the rock but does not extend to the ends of the sample. The fracture splits into two fractures from the middle and propagates to both sides,

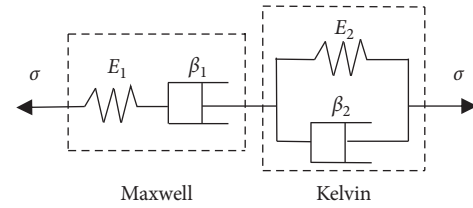


FIGURE 6: Burgers model.

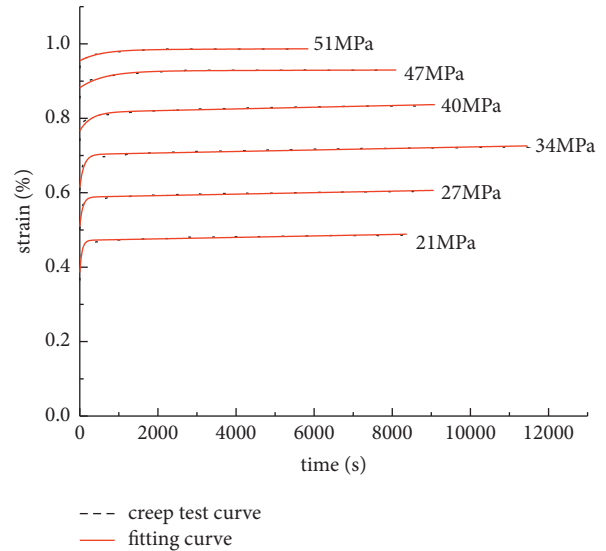


FIGURE 7: Creep curves of various stresses in a dry state.

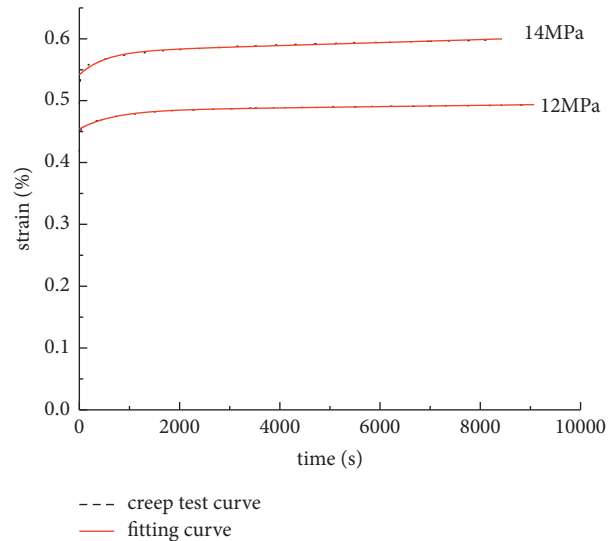


FIGURE 8: Creep curves of various stresses in a saturated state.

forming a “herringbone” shear fracture surface. This failure mode is X-shaped conjugate oblique shear failure, and the shear stress at the failure surface exceeds the strength limit. At the same time, the maximum shear stress sustained by the failure surface before the failure is also related to the positive stress, and it was known as a compression-shear failure. The

TABLE 2: Nonlinear fitting creep parameters of argillaceous red sandstone.

Water content status	Stress/MPa	$E_1/GPa$	$E_2/GPa$	$\beta_1/GPa \cdot s$	$\beta_2/GPa \cdot s$	$R^2$
Drying	21	5.44	24.38	$1.07 \times 10^6$	1401.96	0.935
	27	5.31	33.83	$1.36 \times 10^6$	2555.14	0.939
	34	5.54	38.40	$1.68 \times 10^6$	4089.46	0.944
	40	5.22	80.41	$1.75 \times 10^6$	22650.70	0.939
	47	5.33	103.73	$1.50 \times 10^7$	64030.86	0.940
	51	5.34	177.32	$1.26 \times 10^7$	104305.88	0.918
Saturated	12	2.64	39.77	$1.17 \times 10^7$	27427.59	0.975
	14	2.58	37.37	$5.74 \times 10^5$	19164.10	0.960

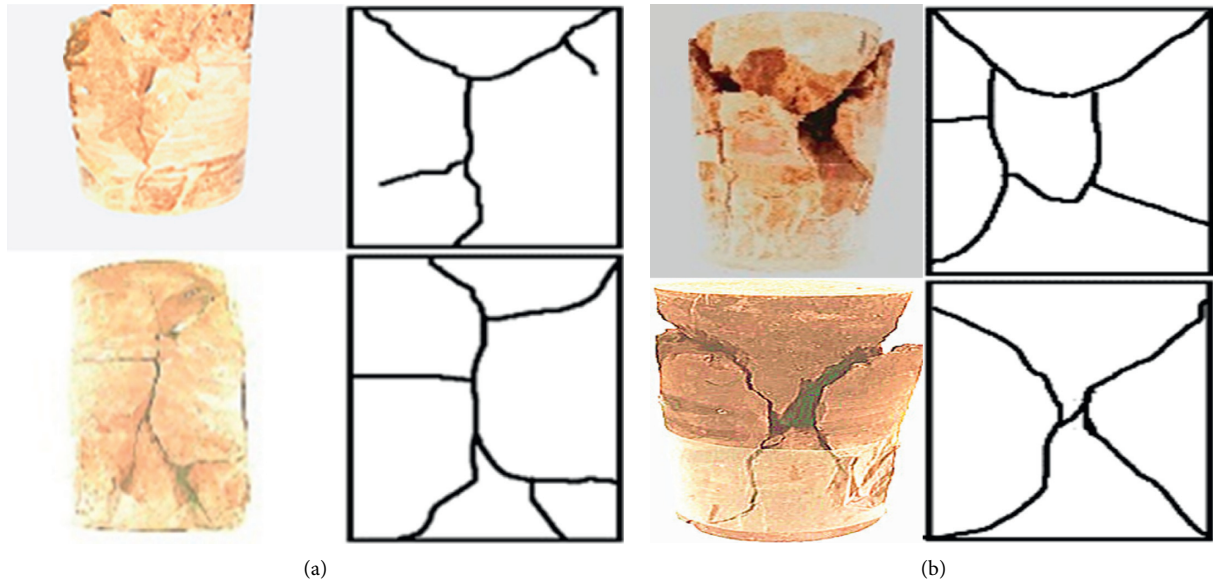


FIGURE 9: Creep failure specimens. (a) Creep failure specimens in dry states. (b) Creep failure specimens in saturated states.

fragments after the destruction of the specimen in the dry state are larger in size and smaller in number. When the specimen is destroyed, only a small amount of powder is generated, while a large crush sound is heard. However, when a saturated specimen was broken, there was no loud sound, and a large amount of debris and powder was produced. This is because the specimen is saturated with water, which dissolves the clay minerals in the rock. As a result, the cementing material is destroyed, and the cementing ability between the internal particles is reduced. And the particles fall off and are failed by external extrusion. At this time, the small particles act as “ball” between the fragments (Figure 10), reducing the friction between the fracture surface and resulting in faster destruction and larger deformation of the specimen.

**5.2. Detailed View Analysis.** There are many rock microscopic analysis methods, most is to scan the rock samples, such as X-ray CT image technology [25, 26], which could be a very good description of the structure characteristics of rock. This paper used MLA650 F type of field emission scanning electron microscopy to scan the sample and got the argillaceous sandstone under different conditions of electron microscopy. Thus, a comparative analysis could be carried out.



FIGURE 10: SEM of fracture in a saturated state.

Four sectional specimens were selected from two different states and different types of test failure specimens. Specimens are carefully cut, and the back of the fracture is polished to make a thickness of about 0.5 cm. Gold was sprayed and placed on the sample stage for electron microscopy scanning. The fine morphology of the specimens with different water content is shown in Figures 11 and 12.

From Figure 12, it can be seen that the number of pores of the specimens after full water are obviously more than the

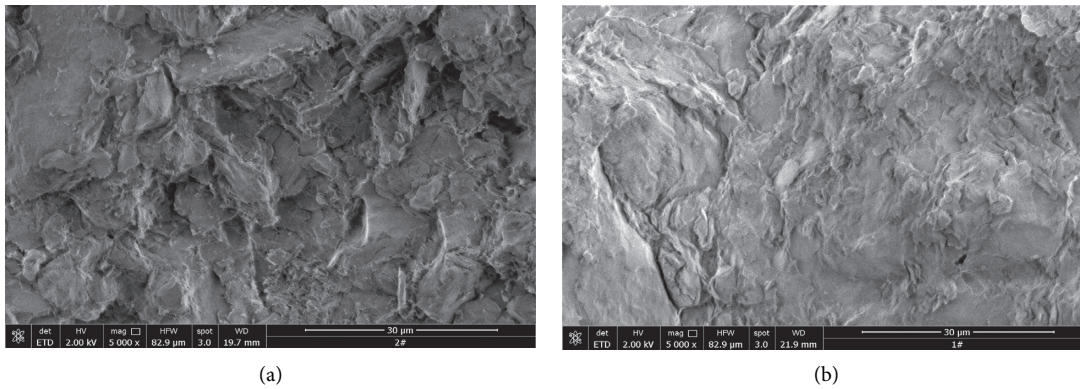


FIGURE 11: SEM of fracture in a dry state. (a) Electron micrograph of Sample 1. (b) Electron micrograph of Sample 2.

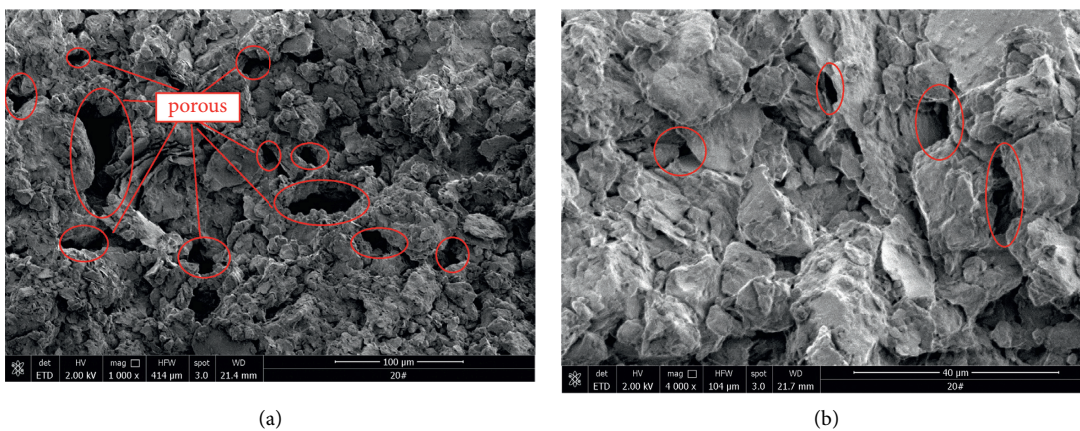


FIGURE 12: SEM of fracture in a saturated state. (a) Electron micrograph of Sample 3. (b) Electron micrograph of Sample 4.

dry state, because of the water pressure, and water enters the fissures so that the fissures are expanding, and the fissures are gradually penetrating each other.

Comparing Figures 11 and 12, it can be seen that the cementation between the particles in the water-saturated state is more loose, and the crystal particles are larger because the clay minerals in the rock are dissolved in water, which weakens the cementation ability between the crystals. At the same time, this makes the particles in the rock swell, so that the strength of the rock sample in the water-saturated state is reduced, and the deformation will be larger than that of the specimen in the dry state under the same stress.

## 6. Conclusion

- (1) The creep deformation of the rock samples under the first level of axial pressure in the dry and water-saturated states is larger than the deformation produced by the increase in stress at any of the later levels, which can reach more than 49% of the ultimate creep at both states. The long-term strengths of muddy red sandstone in the dry and saturated states were calculated to be 46.4 MPa and 14.1 MPa, respectively.
- (2) The rheological mechanical parameters of the burgers model were determined by nonlinear fitting of

creep curves using the burgers model, indicating that the burgers model is applicable to muddy red sandstone.

- (3) The action of water causes rock particles to fall off and acts as a “ball” on the fracture surface, which reduces the friction of the fracture surface and weakens the rock strength. At the same time, the water-filled muddy red sandstone has larger internal pores and lower cementation capacity due to the action of water, which makes it easier for the rock to deform.

## Data Availability

The data presented in this study are available on request from the corresponding author.

## Conflicts of Interest

The authors declare no conflicts of interest.

## Authors' Contributions

S.G. contributed to formulation, writing, and analysis of the paper; S.W. contributed to conceptualization and project

administration; H.F. reviewed and edited the manuscript; H.G. contributed to supervision. All authors have read and agreed to the published version of the manuscript.

## Acknowledgments

This research was funded by the National Natural Science Foundation Project (no. 51978668) (in China).

## References

- [1] Y. Yu, G. L. Feng, C. J. Xu, B. R. Chen, D. X. Geng, and B. T. Zhu, "Quantitative threshold of energy fractal dimension for immediate rock-burst warning in deep tunnel: a case study," *Lithosphere*, vol. 2021, Article ID 1699273, 2022.
- [2] H.-S. Deng, H.-L. Fu, Y. Shi, Y.-Y. Zhao, and W.-Z. Hou, "Countermeasures against large deformation of deep-buried soft rock tunnels in areas with high geostress: a case study," *Tunnelling and Underground Space Technology*, vol. 119, Article ID 104238, 2022.
- [3] P. A. L. P. Firme, D. Roehl, and C. Romanel, "An assessment of the creep behaviour of Brazilian salt rocks using the multi-mechanism deformation model," *Acta Geotechnica*, vol. 11, no. 6, pp. 1445–1463, 2016.
- [4] P. A. L. P. Firme, N. B. Brandao, D. Roehl, and C. Romanel, "Enhanced double-mechanism creep laws for salt rocks," *Acta Geotechnica*, vol. 13, no. 6, pp. 1329–1340, 2018.
- [5] Z. Liu, C. Zhou, B. Li, L. Zhang, and Y. Liang, "Effects of grain dissolution-diffusion sliding and hydro-mechanical interaction on the creep deformation of soft rocks," *Acta Geotechnica*, vol. 15, no. 5, pp. 1219–1229, 2020.
- [6] C. Xia, Z. Liu, and C. Zhou, "Burger's bonded model for distinct element simulation of the multi-factor full creep process of soft rock," *Journal of Marine Science and Engineering*, vol. 9, no. 9, p. 945, 2021.
- [7] A. Lu, X. Chang, S. Hu, X. Yu, and L. Ming, "Impact of moisture content on the brittle-ductile transition and microstructure of sandstone under dynamic loading conditions," *Advances in Civil Engineering*, vol. 2021, Article ID 6690171, 2021.
- [8] S. Okubo, K. Fukui, and K. Hashiba, "Development of a transparent triaxial cell and observation of rock deformation in compression and creep tests," *International Journal of Rock Mechanics and Mining Sciences*, vol. 45, no. 3, pp. 351–361, 2008.
- [9] J. Q. Guo, X. L. Liu, and C. S. Qiao, "Experimental study of mechanical properties and energy mechanism of karst limestone under natural and saturated states," *Chinese Journal of Rock Mechanics and Engineering*, vol. 33, no. 2, pp. 296–308, 2014.
- [10] S. Huang, Y. He, G. Liu, Z. Lu, and Z. Xin, "Effect of water content on the mechanical properties and deformation characteristics of the clay-bearing red sandstone," *Bulletin of Engineering Geology and the Environment*, vol. 80, no. 2, pp. 1767–1790, 2021.
- [11] P. Baud, W. Zhu, and T.-F. Wong, "Failure mode and weakening effect of water on sandstone," *Journal of Geophysical Research: Solid Earth*, vol. 105, no. B7, pp. 16371–16389, 2000.
- [12] F. Wu, H. Zhang, Q. Zou, C. Li, J. Chen, and R. Gao, "Viscoelastic-plastic damage creep model for salt rock based on fractional derivative theory," *Mechanics of Materials*, vol. 150, Article ID 103600, 2020.
- [13] D. Zhang, R. Pathegama Gamage, M. Perera, C. Zhang, and W. Wanniarachchi, "Influence of water saturation on the mechanical behaviour of low-permeability reservoir rocks," *Energies*, vol. 10, no. 2, p. 236, 2017.
- [14] Q. Yao, T. Chen, M. Ju, S. Liang, Y. Liu, and X. Li, "Effects of water intrusion on mechanical properties of and crack propagation in coal," *Rock Mechanics and Rock Engineering*, vol. 49, no. 12, pp. 4699–4709, 2016.
- [15] Y. Wang, L. Cong, X. Yin, X. Yang, B. Zhang, and W. Xiong, "Creep behaviour of saturated purple mudstone under triaxial compression," *Engineering Geology*, vol. 288, Article ID 106159, 2021.
- [16] C. Ping, L. Wan, and Y. Wang, "Viscoelasto-plastic properties of deep hard rocks under water environment," *Transactions of Nonferrous Metals Society of China*, vol. 21, no. 12, pp. 2711–2718, 2011.
- [17] C. Yu, S. Tang, C. A. Tang et al., "The effect of water on the creep behavior of red sandstone," *Engineering Geology*, vol. 253, pp. 64–74, 2019.
- [18] T. Miyazaki, K. Sueyoshi, and T. Hiraga, "Olivine crystals align during diffusion creep of Earth's upper mantle," *Nature*, vol. 502, no. 7471, pp. 321–326, 2013.
- [19] S. Nadimi, K. Shahriar, M. Sharifzadeh, and P. Moarefvand, "Triaxial creep tests and back analysis of time-dependent behavior of Siah Bisheh cavern by 3-Dimensional Distinct Element Method," *Tunnelling and Underground Space Technology*, vol. 26, no. 1, pp. 155–162, 2011.
- [20] H. F. Deng, J. L. Li, and C. J. Deng, "Analysis of sampling in rock mechanics test and compressive strength prediction methods," *Rock and Soil Mechanics*, vol. 32, no. 11, pp. 3399–3403, 2011.
- [21] H. Liu, Z. Li, Y. Zhang, and D. Wang, "The weakening mechanisms of the rock mechanics of marlite bank slopes under water-rock interaction conditions," *Carbonates and Evaporites*, vol. 35, pp. 1–11, 2020.
- [22] N. Zhang, "Interaction between water and soft rocks," *Soft Rock Mechanics and Engineering*, Springer, Cham, Switzerland, pp. 235–249, 2020.
- [23] L. Q. Li, W. Y. Xu, W. Wang, and Y. Q. Guo, "Estimation of long-term strength for Xiangjiaba sandstone based on creep tests," *Engineering Mechanics*, vol. 27, no. 11, pp. 127–136, 2010.
- [24] Y. Zhang, W. Y. Xu, J. F. Shao, H. B. Zhao, and W. Wang, "Experimental investigation of creep behavior of clastic rock in Xiangjiaba Hydropower Project," *Water Science and Engineering*, vol. 8, no. 1, pp. 55–62, 2015.
- [25] W. Lin, X. Li, Z. Yang et al., "A new improved threshold segmentation method for scanning images of reservoir rocks considering pore fractal characteristics," *Fractals*, vol. 26, no. 02, Article ID 1840003, 2018.
- [26] W. Lin, S. Xiong, Y. Liu, Y. He, S. Chu, and S. Liu, "Spontaneous imbibition in tight porous media with different wettability: pore-scale simulation," *Physics of Fluids*, vol. 33, no. 3, Article ID 032013, 2021.